

Supporting Information

Electronic properties of epitaxial cerium oxide films during controlled reduction and oxidation studied by resonant inelastic x-ray scattering

Gabriele Gasperi^{1,2}, Lucia Amidani³, Francesco Benedetti^{1,2}, Federico Boscherini^{4,5}, Pieter Glatzel³, Sergio Valeri^{1,2}, Paola Luches²

¹ Dipartimento di Scienze Fisiche Informatiche e Matematiche, Università degli Studi di Modena e Reggio Emilia, Via G. Campi 213/a, 41125 Modena, Italy

² Istituto Nanoscienze, Consiglio Nazionale delle Ricerche, Via G. Campi 213/a, 41125 Modena, Italy

³ European Synchrotron Radiation Facility, BP 220, F-38043 Grenoble, France

⁴ Dipartimento di Fisica e Astronomia, Viale C. Berti Pichat 6/2, 40127 Bologna, Italy

⁵ Istituto Officina dei Materiali, Consiglio Nazionale delle Ricerche, Operative Group in Grenoble, c/o ESRF, BP 220, F-38043 Grenoble, France

1. XPS characterization

After growth the sample composition and stoichiometry were evaluated in-situ by XPS using an Al K_{α} x-ray source and a hemispherical deflection electron analyzer. In particular, the Ce oxidation state of the films was checked by analyzing Ce 3d XPS spectra. The spectra were fitted using three doublets related to Ce^{4+} ions and two doublets related to Ce^{3+} ions, following the procedures exposed in references [1,2]. Figure S1 shows the data for the 2 and the 10 ML cerium oxide film and the corresponding fit. The spectrum of the 10 ML film was fitted using only Ce^{4+} related components, while the spectrum of the fitting resulted in a Ce^{3+} concentration of approximately 3%, in qualitative agreement with HERFD-XANES spectra in Fig. 2. The partial reduction of ultrathin film is ascribed to charge transfer from the Pt substrate [3], and/or to a larger fraction of low coordinated sites.

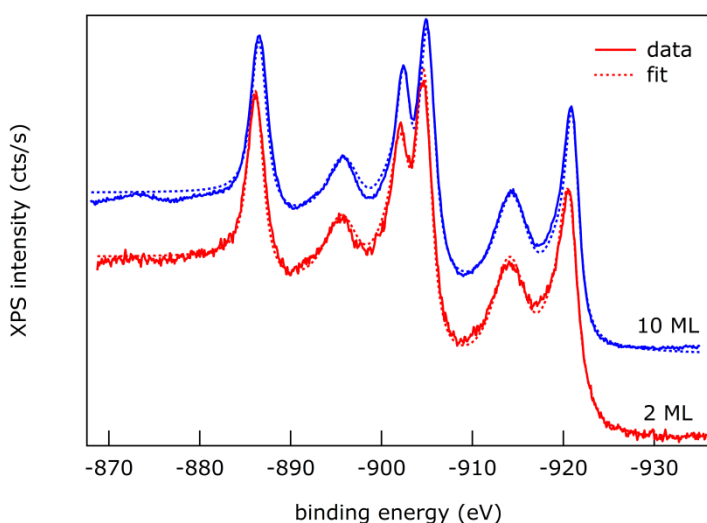


Figure S1: Ce 3d XPS spectra of the 2 and 10 ML cerium oxide films (solid lines) and corresponding fittings (dashed lines).

XPS was also used to cross check the film thickness with the values obtained from the quartz microbalance. We measured the intensities of the Ce 3d and Pt 4f peaks for the two films. For the 2 ML sample we used the values measured before the thermal treatment in oxygen partial pressure, i.e. when the Pt surface was fully covered by the cerium oxide film. Using a simple attenuation model, and assuming the values for the inelastic mean free path evaluated following reference [4] ($\lambda_{\text{Ce}}=13\text{\AA}$; $\lambda_{\text{Pt}}=26\text{\AA}$), it was possible to confirm that the thickness of the nominally 10 ML film is approximately five times the thickness of the thinner film.

2. STM characterization

After growth the samples were also characterized in morphology using STM. The measurements were performed in UHV at room temperature using an electrochemically etched tungsten tip, degassed for 15 minutes at 570 K. Fig. S2 shows the morphology of the 2 ML sample before and after the thermal treatment in oxygen partial pressure. As already observed in previous studies, the sample forms grains of nanometric size after room temperature growth (Figure S2 a), and the thermal treatment induces the formation of flat islands of several tens of nm average lateral size and 2 – 3 ML thickness (Figure S2 b and d) and leaves a fraction of the Pt substrate uncovered. A typical 10 ML film exposes several CeO₂ planes, with protruding structures and holes of a few tens of nm size (Figure S2 c).

The densities of low coordination surface sites on the 2 and 10 ML film were estimated by measuring the density of step edges on STM images like the ones shown in Figure S2 b and c. The average step density results comparable on the two surfaces ($\sim 0.11\text{-}0.15\text{ nm}^{-1}$).

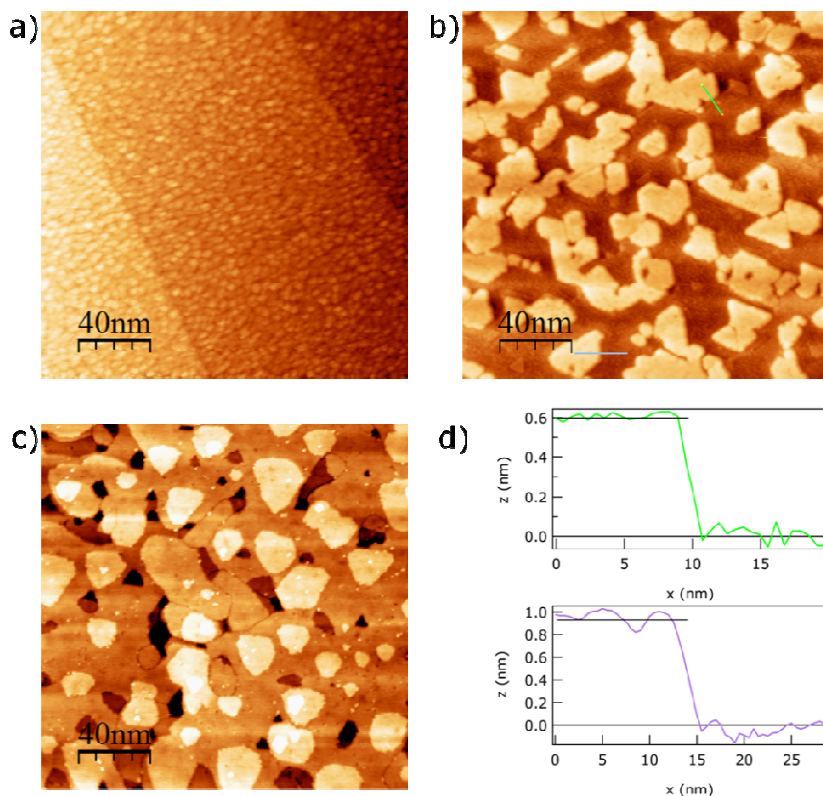


Figure S2: STM images of: a) the 2 ML film as grown at room temperature ($V=3\text{ V}$, $I=0.03\text{ nA}$); b) the 2 ML ($V=1.2\text{ V}$, $I=0.04\text{ nA}$) and c) a 10 ML ($V=3\text{ V}$, $I=0.1\text{ nA}$) film after the thermal treatment in $P_{\text{O}_2}=1\times 10^{-7}\text{ mbar}$ at 1040 K. d)

Height profiles along the lines evidenced in b) showing that the height of the cerium oxide islands on the 2 ML film is 2 - 3 ML (i.e. $\sim 6 - 9 \text{ \AA}$).

3. LEED characterization

LEED patterns were acquired in-situ after the growth to have information on the surface structure of the samples. The incident electron energy used was 80 eV. Sharp cerium oxide and Pt related spots are evident in the LEED pattern of the 2 ML film (Figure S3 a). The Pt spots originate from uncovered Pt surface areas. In the 10 ML film, instead, only the spots related to the CeO_2 film are evident (Figure S3 b). The symmetry and the sharpness of the spots indicate a well-ordered (111) orientation of the film surfaces.

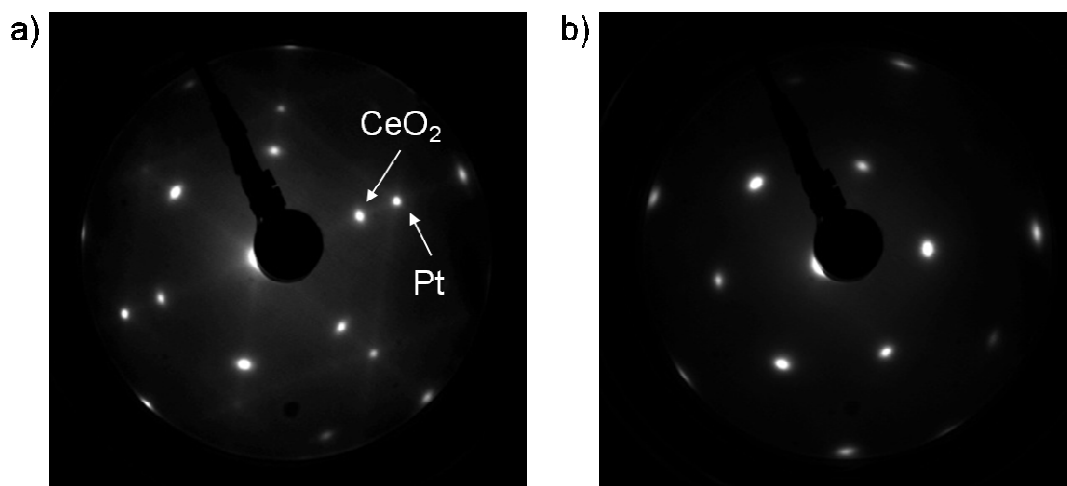


Figure S3: LEED patterns of the 2 ML (a) and 10 ML (b) CeO_2 film measured after room temperature growth and thermal treatment in oxygen partial pressure.

4. Beam irradiation damage

We investigated the possible modifications of the cerium oxidation state induced by photon beam exposure in the 2 ML sample. The incident photon flux was of the order of 10^{12} ph/s at 5725 eV. Each stage of the reducing/oxidizing cycle was characterized by taking HERFD-XANES for approximately an hour. We did not detect any significant change in the spectra during exposure times comparable to the ones used for acquisition of HERFD-XANES spectra (approximately 1 h). Anyway the effects of the reducing/oxidizing cycle are by far stronger than the small effects induced by one hour beam exposure. Prolonged exposure to the beam instead induced detectable modifications in the shape of the spectra. Figure S4 reports a HERFD-XANES spectrum of the 2 ML CeO_2 film as introduced in high vacuum (HV) and a second spectrum acquired after approximately 6 h of continuous beam exposure (RIXS plane acquisition). It is possible to notice that beam exposure in high vacuum causes a mild reduction. The modifications are however minimal compared to the ones induced by the vacuum thermal treatments shown in Figure 2 a. Moreover, it has to be pointed out that the changes of the oxidation state induced by the photon beam were found to be dependent on the initial oxidation state of the sample. Fig. S4 also reports a HERFD-XANES spectrum of the 2 ML CeO_2 film after the thermal treatment in HV, i.e. in the fully reduced state, and a second one acquired after 6 h of continuous beam exposure. In this case

the beam induces a mild oxidation of the sample. To avoid areas damaged by the beam, the sample was shifted by a few tenths of mm after each long acquisition.

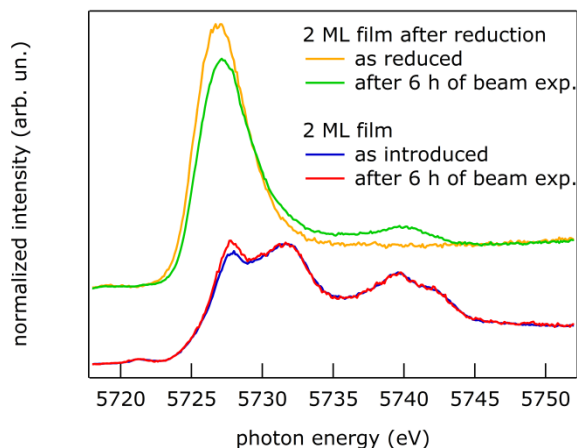


Figure S4: Ce L₃-edge HERFD-XANES of the 2 ML film cerium oxide film: as introduced (blue line), after 6 h of beam exposure (red line), after reduction by heating at 1020 K in HV (yellow line) and after reduction plus 6h of beam exposure (green line).

5. Principal component analysis

To determine the number and the nature of spectral components which contribute to the HERFD-XANES spectra during reduction and oxidation, we performed a principal component analysis of the spectra. The first step consisted in identifying the minimum number of spectrally different components, necessary to reproduce each spectrum within the experimental error. This was done by the Sixpack program [5], using the semiempirical indicator function IND, introduced by Malinowski [6]. The function for the full set of spectra (Figure S5 a) shows a marked decrease for two components and it significantly increases only above 10 components. The second step is the identification of the two spectrally different components which contribute to the spectra. We chose the two extreme spectra in reducing and oxidizing conditions, i.e. the spectrum of the 2 ML sample at 1020 K in HV (Ce³⁺ reference) and the spectrum of the 10 ML sample at 1020 K in O₂ (Ce⁴⁺ reference). After removal of these two spectra, the IND function shows a similar trend as the one observed including all the spectra and it has an identical value for two components. This indicates that the choice of the two mentioned spectra as principal components is correct. The procedure gave very similar results for the spectra in the pre-edge region (Figure S5 b). The results from PCA strengthen the interpretation of both main-edge and pre-edge HERFD-XANES spectra as a linear combinations of the chosen Ce³⁺ and Ce⁴⁺ spectral components at the different stages of reduction/oxidation.

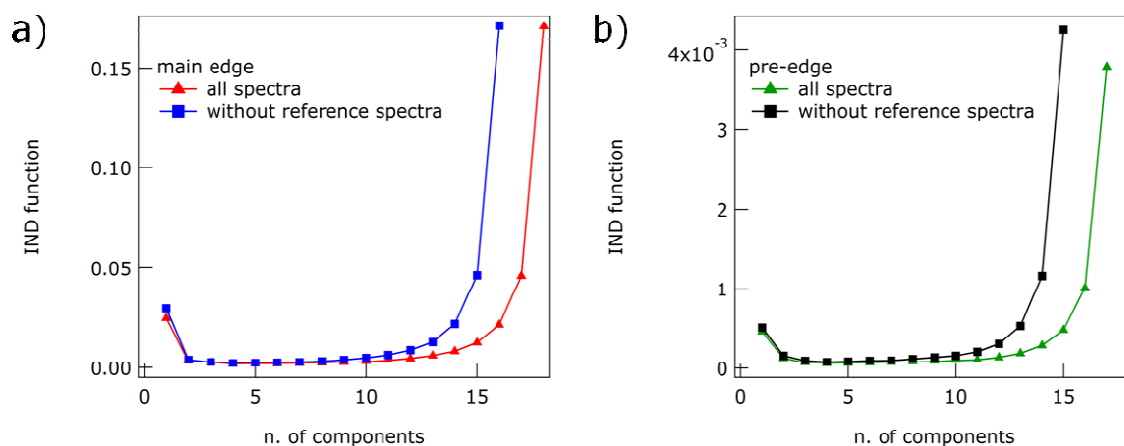


Figure S5: a) IND function for different number of components considering the whole set of HERFD-XANES spectra with (red triangles) and without (blue squares) the spectra chosen as references, i.e. the spectrum of the 2 ML sample at 1020 K in HV (Ce^{3+} reference) and the one of the 10 ML sample at 1020 K in O_2 (Ce^{4+} reference); b) IND function as in a) for the HERFD-XANES spectra in the pre-edge region.

6. Size effects in HERFD-XANES

Figure S6 shows the spectrum of the 2 ML film at room temperature after the full cycle in oxygen, i.e. in a condition in which the density of oxygen vacancies is expected to be minimum.

The green spectrum is a linear combination of the spectrum of the 10 ML spectrum at room temperature after the full cycle in oxygen and of the 2 ML film at RT after the full HV cycle, weighted by 0.95 and 0.05 respectively. The two components are also shown in black in figure S6. The edge position and relative intensities of the features at 5728 and 5732 eV are reproduced satisfactorily, while minor differences can still be observed. This shows that the main effect of vertical confinement can be described as the formation of Ce^{3+} sites, consistent with the charge transfer from the platinum substrate to the oxide already observed in the same system [3].

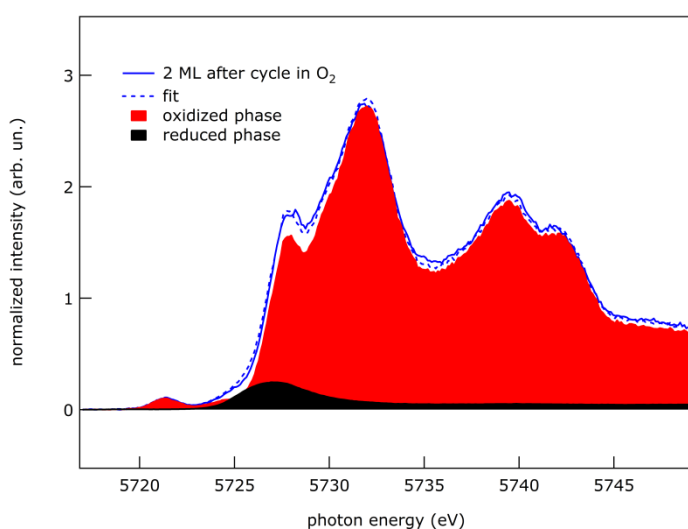


Figure S6: Ce L_3 -edge HERFD-XANES spectra of the 2 ML film at room temperature after the full cycle in oxygen (blue solid curve), linear combination of the spectrum of the 2 ML film at RT after the full HV cycle (reduced phase) and of the 10 ML spectrum at room temperature after the full cycle in oxygen (oxidized phase), weighted by 0.05 and 0.95 respectively (blue dashed curve). The two components are also shown in red and black.

References

- [1] T. Skála, F. Šutara, M. Škoda, K. C. Prince, and V. Matolín, *Journal of Physics: Condensed Matter* **21**, 055005 (2009).
- [2] P. Luches, F. Pagliuca, and S. Valeri, *J Phys Chem C* **115**, 10718 (2011).
- [3] P. Luches *et al.*, *Adv Mater Interfaces*, n/a (2015).
- [4] S. Tanuma, C. J. Powell, and D. R. Penn, *Surface and Interface Analysis* **25**, 25 (1997).
- [5] S. M. Webb, *Physica Scripta* **2005**, 1011 (2005).
- [6] E. R. Malinowski, *Analytical Chemistry* **49**, 612 (1977).